A GIS-BASED ASSESSMENT METHOD FOR MEAN RADIANT TEMPERATURE IN DENSE URBAN AREAS

Jianxiang Huang, [1] Jose Guillermo Cedeño Laurent, [2] John Spengler, [3] Christoph Reinhart [4]

[1]Harvard University Graduate School of Design, Cambridge, MA

[2]Harvard University School of Public Health, Boston, MA

[3]Harvard University School of Public Health, Boston, MA

[4]The Massachusetts Institute of Technology Department of Architecture, Cambridge, MA

ABSTRACT

The mean radiant temperature (T_{mrt}) is among the most important factors affecting thermal comfort. Its assessment in dense cities has been complicated due to the presence of buildings, pavings, and infrastructure. This paper introduced the RAMUM model, a GIS based software method developed to simulate outdoor mean radiant temperature at micro-scale. The advantages of this method lie in its efficiency and resolution that supports the design of buildings, streets, and public open spaces. The model is evaluated using field measurements under cold and warm weather in Boston. This study is sponsored by the EFRI-1038264 award from the National Science Foundation (NSF), Division of Emerging Frontiers in Research and Innovation (EFRI).

INTRODUCTION

The mean radiant temperature (T_{mrt}) is among the most important meteorological factors in relation to human body energy balance. It is by definition the uniform temperature of an imaginary enclosure in which radiant heat transfer from the human body is equal to the radiant heat transfer in the actual non-uniform enclosure (ISO, 1998). It is a key variable to thermal comfort and pedestrian activities (Nikolopoulou and Lykoudis, 2006), which are essential to the design of walkable and livable cities that promotes health and sustainability. There is a practical need for environmental assessment tools that are both efficient and supportive of design decisions at micro-scale.

The objective of this paper is to present a software method to simulate T_{mrt} in urban environments. The model is named the Rapid Assessment Method for Urban Microclimate (RAMUM). It is based on ArcGIS, the widely used data platform among researchers and design practitioners. The model requires minimum input of dry bulb temperature, relative humidity, 3D buildings and topography information. It is capable of computing T_{mrt} for two-dimensional surfaces at a grid resolution of one meter by one meter, and the results can be graphically interpreted on hourly basis. The model is evaluated using field measurements conducted in Boston, Massachusetts.

LITERATURE

The assessment of T_{mrt} has been complex in dense urban areas, since both shortwave and longwave radiations are highly varied due to the presence of buildings, infrastructure, and paving. Several tools emerged in recent years in an attempt to simulate radiation influx at the urban scale. Rayman Pro is a software tool designed for outdoor environmental analysis. The software is based on a stationery heat balance model, and it takes into account both short-wave and long-wave radiation fluxes (Matzarakis, 2007). It requires separate morphological input, and it can neither process complex building geometries nor calculate T_{mrt} on a continuous surface. Similarly, ENVI-met is a software package capable of simulating the surface-plant-air interactions in urban environments. The software applies computational fluid dynamics (CFD) models and energy balance models (Bruse, 2006). Like Rayman Pro, ENVI-met is limited in data input and complex geometries. Others include the Simulation Platform of Thermal Environment (SPOTE) (Lin, et al., 2006), the Townscope II (Teller and Azar, 2001), and the Integrated Environmental Solutions – Virtue Environment (IES, 2012).

Despite the rising importance in sustainable design and occupant comfort, environmental assessment tools are rarely used in planning and urban design practices. Barriers persist between researcher and practitioners,

and existing tools are often limited in model input, data exchange, and visualization capacities. To better serve the needs of urban designers and planners, the simulation model should be computationally efficient, transparent, and graphically intuitive. It should support information exchange with other simulation packages as well as database platform such as the Geographic Information System (ESRI, 2012), a widely used software among design practitioners.
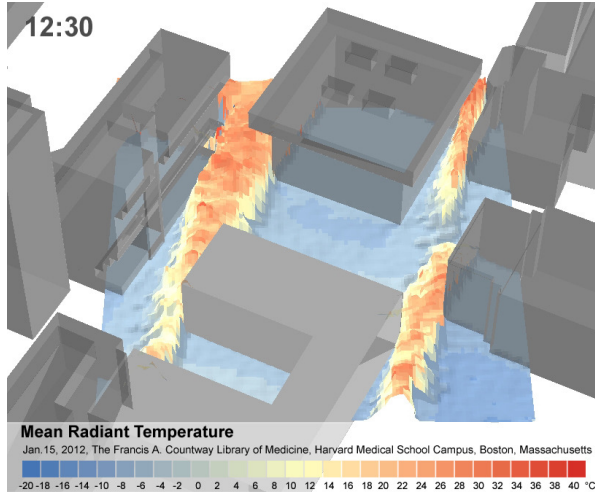

Figure 1. The mean radiant temperature at 1.5 meters height above ground

METHOD

By definition, the calculation of T_{mrt} can be expressed with the following formula (Fanger, 1970)

$$T_{mrt} = \sqrt[4]{(\varepsilon_1 \cdot T_1^4 \cdot F_{p\text{-}1} + \varepsilon_2 \cdot T_2^4 \cdot F_{p\text{-}2} + \ldots + \varepsilon_n \cdot T_n^4 \cdot F_{p\text{-}n})}$$

(1)

$\varepsilon_n =$ Emittance for surface materials (ratio)
$T_n =$ Temperature of isothermal surfaces
$T_n =$ View factor of isothermal surfaces

In real urban context, it is impractical to estimate temperature for every isothermal surface. A simplified approach separates radiation into three components: shortwave radiation; longwave radiation from the sky; and longwave radiation from solid surfaces, in this case the ground and the buildings. The alternative formula is presented below and the calculation for each of the three components will be explained in detail.

$$T_{mrt} = \sqrt[4]{\frac{1}{\sigma}(a_k \cdot E_s \cdot F_s + \varepsilon_p \cdot E_a \cdot F_a + \varepsilon_p \cdot E_g \cdot F_g)}$$

(2)

$\sigma =$ Stephan-Bolzmann Constant
        $(5.67 \cdot 10^{-8} \ W/m^2 K^4)$

$a_k =$ Absorption coefficient of shortwave radiation for the target object (standard value 0.7)
$\varepsilon_p =$ Emission coefficient for the target object (standard value 0.97)
$E_a =$ Longwave radiation intensity of the open sky (W/m^2)
$E_n =$ longwave radiation intensity of solid surfaces (W/m^2)
$F_{s,a,g} =$ angle factors of the sky, solar radiation, and solid surfaces (ratio)

The target object for this study is a 40mm grey ball thermometer placed at 1.5 meter above the ground, an approximate of human body. The model also uses weather data from the nearest station, in this case the portable weather station present on site is brought into use. The workflow is automated using the programming language of Python. The results are presented in ArcScene at a grid resolution of one meter by one meter. (Figure 1)

Shortwave Radiation

Shortwave radiation can be simulated using DIVA-for-Rhino 2.0 (Jakubiec and Reinhart, 2011), an advanced daylight simulation tool based on Radiance, Daysim (Reinhart and Walkenhorst, 2001) and Rhinoceros 10 interface (McNeel, 2012). The hourly radiation data is downloaded from the Central Square weather station located in Cambridge, MA (Wview, 2012) Three-dimensional urban models of the study area are acquired from Boston Redevelopment Authority (BRA, 2011).

DIVA-for-Rhino calculates hourly the global horizontal irradiance for sensor grids of one meter by one meter. The results are imported to raster layers in ArcGIS. The base map information, including building footprint, road, are acquired from the Office of Geographic Information (MassGIS, 2011).
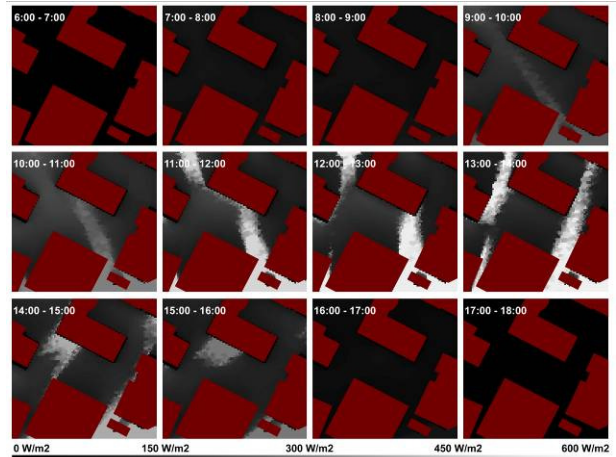
Figure 2, Shortwave radiance E_s of 1m grid resolution, reflectance = 0.35. Hourly calculation conducted using DIVA-for-Rhino Plug-in, based on 3D urban model acquired from the Boston Redevelopment Authority and Massachusetts Office of Geographic Information.

Notice that DIVA-for-Rhino calculates global horizontal radiance received from a planar surface facing upwards. For a spherical surface, the results can be approximated with homogeneous radiation with the angle factor F_s= 0.5. The percentage of error is expected to increase when the solar angle is low. Yet the absolute error will become negligible compared with intrinsic errors imbedded in solar radiation simulation models at low-solar angles (Ibarra and Reinhart, 2011)

Longwave Radiation from the Sky
The radiation from the sky can by estimated using the Angstrom formula: (Falkenberg and Bolz 1949;Monteith 1990; Oke 1987; VDI 1994):

$$E_a = \sigma \cdot (T_a + 273.15)^4 \cdot (0.82 - 0.25 \cdot 10^{-0.0945 V_p}) \cdot (1 + 0.21 (\frac{N}{8})^{2.5})$$

(3)

$E_a =$ Longwave radiation from the sky (W/m^2)
$T_a =$ Dry bulb temperature (°C)
$N =$ Degree of cloudiness (octas)
$V_p =$ Vapor pressure (hPa)

The vapor pressure V_p is computed using Arden Buck equation (Buck,1981)

$$V_p = R_{hum} 6.1121 \cdot \exp((18.678 - \frac{T_a}{234.4}) \cdot (\frac{T_a}{257.14 + T_a}))$$

(4)

$V_p =$ The saturation vapor pressure in hPa
$R_{hum} =$ Relative humidity (%)
$T_a =$ Dry bulb temperature (°C)

For spherical surface, the angle factor of longwave radiation from sky can be conveniently determined from sky view factor

$F_a =$ SVF / 2
SVF = Sky view factor from the center of the grid cell

The sky view factor can be calculated from DIVA-for-Rhino plug-in based on Radiance. Ambient bounces were set equal to one (ab = 1) and run a daylight factor simulation for grid sensors under the uniform sky. The result is imported to ArcGIS using Python programming language. (***Figure 3***)
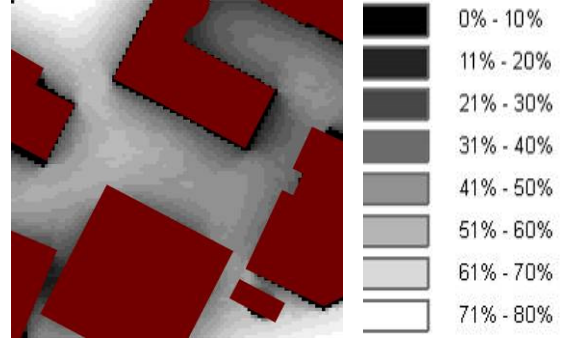

Figure 3. Sky View Factor, calculated using DIVA-for-Rhino Plug-in, plotted from ArcGIS

Longwave Radiation from Solid Surfaces
The longwave radiation from the ground and buildings is determined by aggregate longwave radiation from each isothermal surface as well as those reflected from the sky:

$$E_g = \left[\frac{\sum_{i=1}^{n} (E_i + (1 - \varepsilon_i) \cdot E_a) \cdot F_i}{\sum_{i=1}^{n} F_i} \right]$$

(5)

$E_i =$ longwave radiation from surface (W/m^2)
$\varepsilon_i =$ Emittance of surface material
$E_a =$ Longwave radiation from the sky (W/m^2)
$F_i =$ Angle factor of solid surface (ratio)

The longwave radiation emitted by individual surfaces can be expressed by Stephan-Bolztmann's law:

$$E_i = \varepsilon_i \cdot \sigma \cdot T_s^4$$

σ = Stephan-Bolzmann Constant $(5.67 \cdot 10^{-8}$ W/m^{2}K$^4)$
ε_i = Emittance of surface material,
T_s = Temperature of solid surface

The temperature of solid surfaces, in this case building facades and ground paving, is jointly determined by air temperature, ambient radiation, indoor temperature, and the insulation value of surface materials. The building façades on site consist mostly of stone and concrete surfaces, which reduces uncertainties associated with longwave radiation through glazing.

Infrared photographs were taken at each hour to record solid surface temperatures of the ground and building façade. data suggests that the temperature of individual surfaces could vary up to 20 degrees from the air temperature. However, the mean temperature of all solid surfaces matches closely with the air temperature with small margins of error (*Figure 4*). For simplification purposes, it is therefore reasonable to assume isothermal conditions for all solid surfaces in

the model with temperature equal to those of the ambient air. Given $T_s = T_a$, and for most building materials $\varepsilon \approx 1$, a simplified formula can be expressed below

$$E_g = \sigma \cdot T_a^4 \qquad (6)$$

σ = Stephan-Bolzmann Constant
$\qquad (5.67 \cdot 10^{-8} \text{ W/m}^2\text{K}^4)$
T_a = Dry bulb temperature (°C)

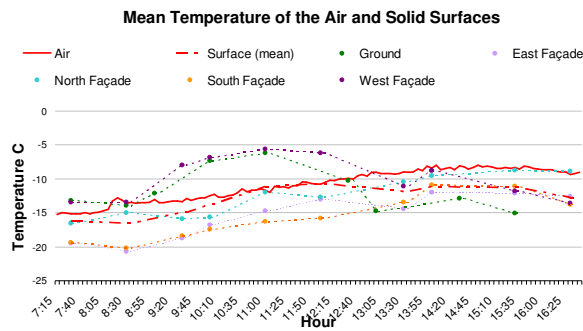**Mean Temperature of the Air and Solid Surfaces**

Figure 4, the air temperature of the dry bulb matches closely with the average temperature of solid surfaces. Façade/ground temperature estimated using hourly infrared photography (Figure 10).

MEASUREMENT

The above simulation results are evaluated using field measurement conducted on January 15 and March 21, 2012 respectively. These experiment dates are chosen to maximize temperature range. The former, Jan.15 is a cold day with low air temperature recorded from -18 to -8 degrees centigrade. In contrast, March 21 is an exceptionally warm day with recorded air temperature betwen 15 and 25 degrees centigrade during the day. Both days are mostly clear except for a few hours of cloudiness in the afternoon of Jan.15.
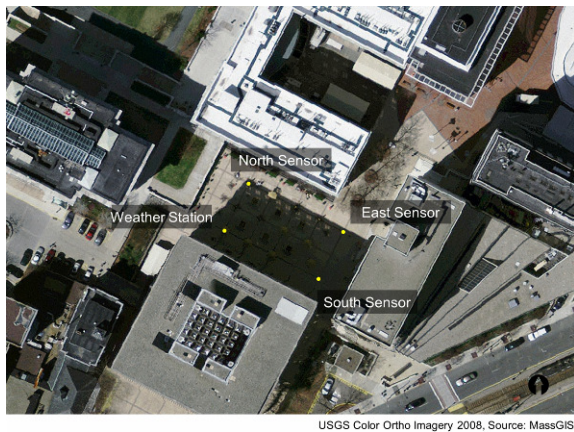
Figure 5. Measurement Site, Countway Library Courtyard, Harvard University, Boston, MA

Equipment in use includes three Onset Temperature Sensor (TMC6-HA), one Wind Speed & Direction Sensor (S-WCA-M003), Silicon Pyranometer Sensor(S-LIB-M003), Barometric Pressure Sensor (S-BPB-CM50), Temp/RH Sensor (S-THB-M002), Hobo data logger (U12-006)

Figure 6, Measurement Devices in use including 38mm Greyball Thermometer, portable weather station, and infrared camera.

Environmental measurements were obtained at four different points of the courtyard in order to assess the possible thermal comfort distribution of occupants in an open space. In Position 1, a micro-weather station (Onset Computer Corporation) equipped with sensors for air temperature, relative humidity, wind speed and direction and solar radiation was used. The readings were recorded at 5-minute intervals to smooth the sudden variations mostly in wind speed and solar radiation due to wind gusts and sunshine/shade variations, respectively. In the other three locations, 40 mm flat grey globe thermometers were used to measure globe temperature. These consist of 40 mm flat grey painted copper balls attached to 4-channel temperature U-12 data loggers (Onset Computer Corporation) recording data also every 5 minutes. Initially used to represent the convective and radiative heat transfer of a human with its surroundings, the use of the smaller diameter globe thermometers has been validated for both indoor and outdoor thermal comfort measurements. The use of a smaller diameter globe with a lower thermal inertia allows the temperature measurements to respond quickly to changes in wind velocities and solar radiation levels usually encountered in outdoor settings. Its use to calculate the mean radiant temperature (T_{mrt}) in open spaces has proved satisfactorily when compared with the T_{mrt} values derived from three-dimensional short-wave and long-wave radiation patterns measured with an expensive arrangement of radiometers and complex view factor calculations. After adjusting for a proper mean convective coefficient, the T_{mrt} obtained values seem to improve the fit with more complex models even further (Thorston, 2007).

To compensate for the convective and conductive heat losses from 40 mm grey ball thermalmeter to the air, the following formula is used to adjust for globe thermometer reading. (Kuehn, 1970)

$$T_{mrt} = \sqrt[4]{(T_g + 273.15)^4 + \frac{1.1 \cdot 10^8 \cdot V_a^{0.6}}{\varepsilon \cdot D^{0.4}} \cdot (T_g - T_a)} - 273.15$$

(7)

T_g =   Globe Temperature (°C)
V_a =   Wind speed (m/s)
T_a =   Air Temperature
D =   Globe diameter (40mm)
ε =   Globe Emittance, 0.97

This inexpensive solution of using globe temperature measurements has also proven to be a good predictor of outdoor thermal comfort. A multinational study performed in several European cities (Nikolopoulou and Lykoudis, 2006) found the correlation between the globe temperature and the Actual Sensation Vote (ASV) responses of study participants to be the highest among all environmental measurements recorded (R=0.53), when compared to air temperature (R=0.43), solar radiation (R=0.23) and wind speed (R=0.26). These studies confirm the usefulness of the globe thermometers to approximate the heat transfer of individuals with the built environment in open spaces.

UNCERTAINTIES

The simulated and measured T_{mrt} during the experiment are plotted in figure 7. The 157 pairs of data entries feature a correlation coefficient of 0.964, while the differences are normally distributed (**Figure 8**). A further breakdown shows the simulation tends to overestimate the T_{mrt} by 1~2°C during warm weather and underestimate the T_{mrt} by 1~2°C during cold weather. The sources of uncertainties stem from building geometries, surface temperature variations, and measurement errors.

A major source of uncertainties is from the 3D building database. Different from the simplifed building geometries in the GIS database, architectural details such as exterior wall profile, windows extrution, androof top structures can change the shape of shadows, resulting in a shift of peak value as it is observed in figure 12 and 13. Many of the outlyers in figure 7 with up to 20°C differences between measurement and prediction can be explained by this cause.
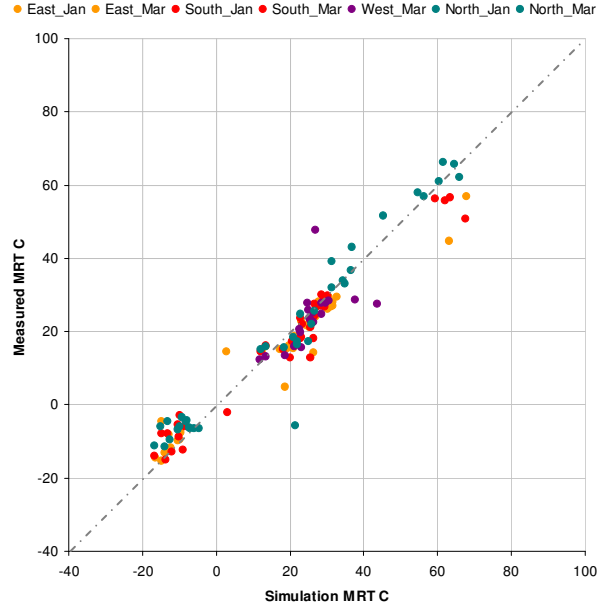

Figure 7. Scatter Plot of Measured T_{mrt} against Predicated T_{mrt} on both Jan. 15 and Mar.21, 2012. Measurement interval = half hour. Observations n = 157; Correlation coefficient r = 0.964
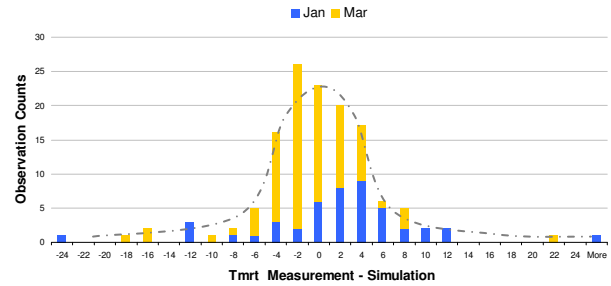

Figure 8, the distribution of differences between measured and predicted T_{mrt} on Jan.15 and Mar.21

A second source of uncertainties comes from temperature variation of solid surfaces, mostly due to solar exposure, thermal bridges, or glazing. Figure 9 presented an estimation of the T_{mrt} in square-shaped courtyard resembling the countway library site. Calculation using Fanger's formula above yeilded a T_{mrt} difference of 1.2°C, a noticable but minor error compared with other sources of uncertainties. Assume global horizontal shortwave radiation to be 600 W/m² and the longwave radiation from the sky to be 200 W/m². The surface temperature of the two solid wall (highlighted in red) are allowed to vary by 10°C higher than those of the others.
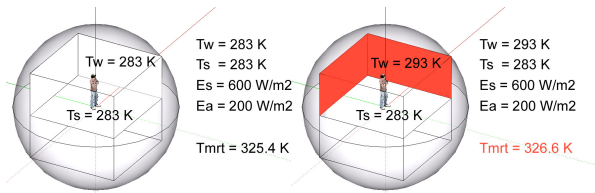
Figure 9, the heated wall surfaces can raise the T_{mrt} by 1.2 °C. The calculation is based on a courtyard space enclosed by walls and floor with a sky view factor of 0.33 from the center. The left scenario assume an equal temperature to all solid surfaces, while the right scenario allows the surface temperature of two solid wall surfaces to rise by 10 °C, the typical differences observed during the experiment.

Aside from simulation uncertaities, measurement are also vulnerable to errors from equipment such as the greyball thermometers. These errors may be further amplified by Kuehn's formula when adjusting for convective heat losses. Further field measurement work are scheduled in order to test the model's applicability in hot climate and under complex weather conditions.

CONCLUSION

The simulation-based method is a useful tool for estimate radiation fluxes at a spatial resolution that informs design deicisions. It is capable of performing rapid analysis in two dimensional. The method requires minimum input of GIS geospatial information as well as meteological data. Since the T_{mrt} is a key estimator of thermal comfort in outdoor space, this simulation method will become a useful tool for design and planning practices. It allows early-phase diagnosis of undesirable radiant fluxes, which will later inform choices on building envelope, shading devices, and vegetation. It can also inform the seleciton of building and paving materials based on thermal properties, the reflectance, emittance, and heat capacity. The model will also support decisions on whether radiant heating or cooling are needed during extreme weather events.

A following application of the model is to calculate outdoor thermal comfort in dense urban spaces. The T_{mrt}, along with wind speed, air temperature, and humidity, constitutes the key meteological inputs for thermal comfort metrics.

REFERENCES

McNeel, R. 2010. Rhinoceros - NURBS Modeling for Windows (version 4.0), McNeel North America, Seattle, WA, USA. (www.rhino3d.com/)

ASHRAE. 2001. ASHRAE Fundamentals Handbook 2001 (SI Edition) American Society of Heating, Refrigerating, and Air-Conditioning Engineers, ISBN: 1883413885.

Azar S. 2006. TownScope III, University of Liege, Belgium. http://www.townscope.com.

Buck, A. L. 1981, "New equations for computing vapor pressure and enhancement factor", J. Appl. Meteorol. 20: 1527–1532

Bruse M. 2006. ENVI-met 3 – a three dimensional microclimate model. Ruhr Universit¨at Bochum, Geographischer Institut, Geomatik. http://www.envi-met.com

ESRI, The GIS software. http://www.esri.com/

Fanger, P.O. 1970, Thermal Comfort: Analysis and Applications in Environmental Engineering, McGraw-Hill Book Company, New York.

Ibarra, Diego; Reinhart, Christoph, 2011, Solar availability: A comparison study of irradiation distribution methods, Building Simulation 2011, Sydney, Australia.

Integrated Environment Solutions: http://www.iesve.com/

International Organization for Standardization, 1998. Ergonomics of the thermal environment - Instrument for measuring physical quantities. Geneva, Switzerland. ISO 7726.

Jakubiec, J A; Reinhart, C F "DIVA-FOR-RHINO 2.0: Environmental parametric modeling in Rhinoceros/Grasshopper using Radiance, Daysim and EnergyPlus", Conference Proceedings of Building Simulation 2011, Sydney, Australia.

Kuehn LA, Stubbs RA, Weaver RS. 1970. Theory of the globe thermometer. Journal of Applied Physiology 29: 750–757.

Lagios, K; Niemasz, J and C F Reinhart, 2010, Animated Building Performance Simulation (ABPS) - Linking Rhinoceros/Grasshopper with Radiance/Daysim, the Proceedings of SimBuild 2010, New York

Lin, Borong; Zhu, Yingxin; Li, Xiaofeng; Qin, Youguo; 2006, Numerical simulation studies of the different vegetation patterns' effects on outdoor

pedestrian thermal comfort. The Forth International Symposium on Computational Wind Engineering, Yokohama, Japan

Nikolopoulou, M. and Lykoudis, S., 2006. Thermal comfort in outdoor urban spaces: Analysis across different European countries. Building and Environment, 41 (11), pp. 1455-1470.

Reinhart C. F. and Walkenhorst O. (2001) Validation of dynamic RADIANCE-based daylight simulations for a test office with external blinds. Energy and Buildings 33, 683-697.

Steel,Mark,2011,wview:http://www.wviewweather.com

The Boston Redevelopment Authority, http://www.bostonredevelopmentauthority.org/Home.aspx

The Common Wealth of Massachussetts, Office of Geographic Information (MassGIS) http://www.mass.gov/mgis/massgis.htm

Thorsson,S., Lindberg, F., Eliasson, I., and Holmer, B., 2007. Different methods for estimating the mean radiant temperature in an outdoor urban setting. International Journal of Climatology, 27, pp.1983–1993
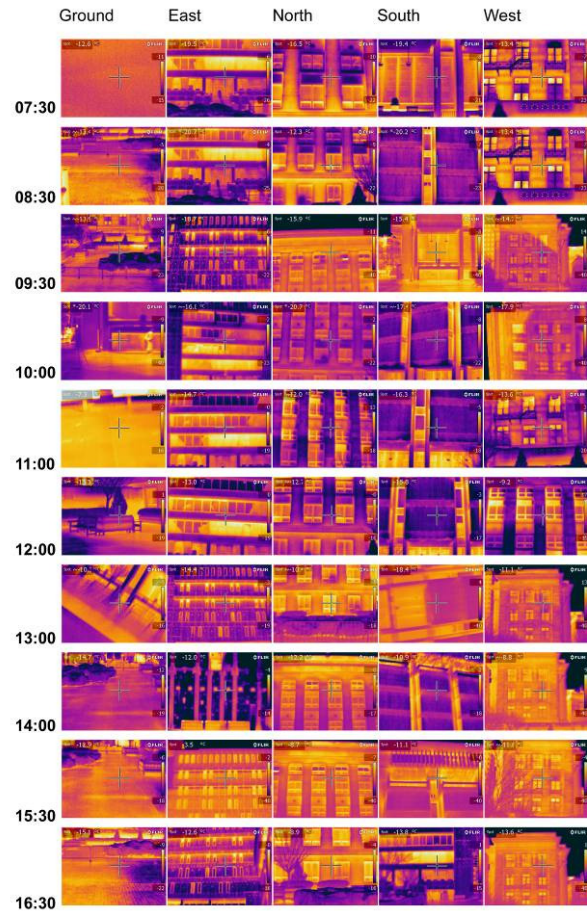
APPENDIX A

Figure 10, Hourly temperature of solid surfaces based on infrared photograph, January 15, 2012
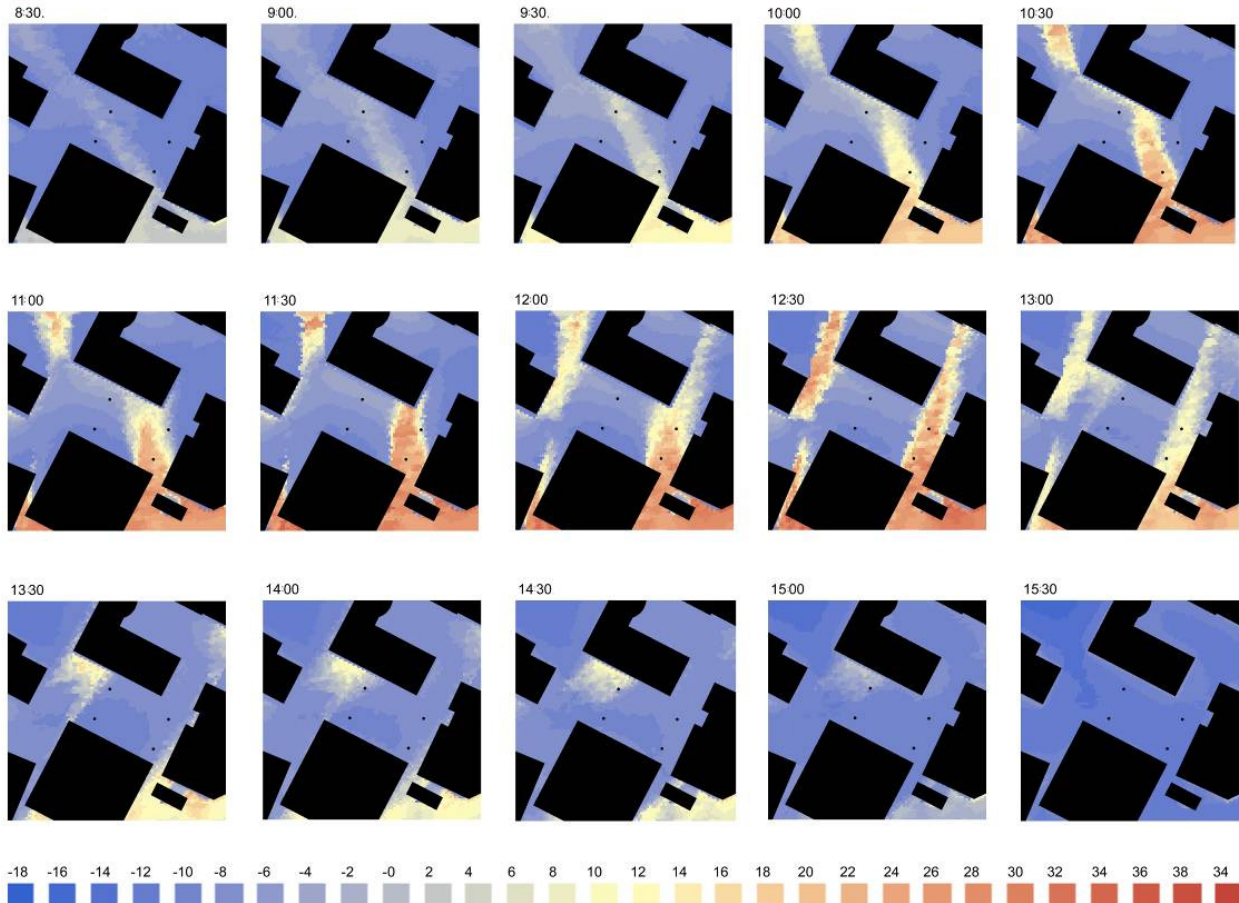
Figure 11. Simulation of Mean Radiant Temperature on Countway Library Courtyard, January 15, 2012. Grid dimension, 1m by 1m. For concrete façade and pavings materials, albedo = 0.35, emissivity = 1
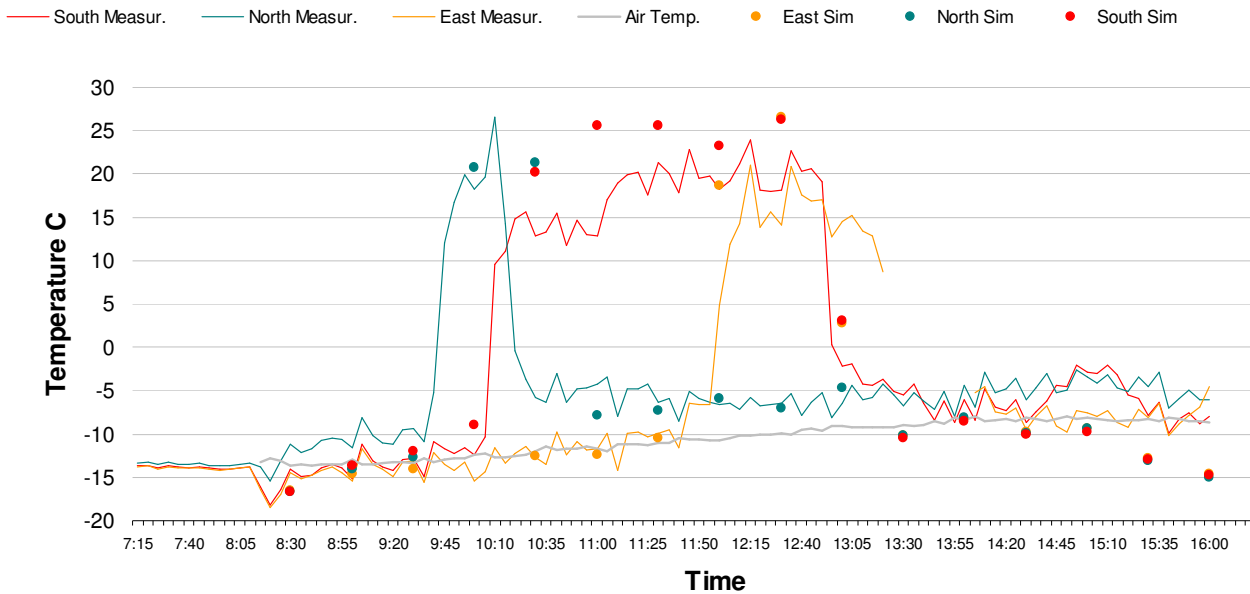

Figure 12. Predicted and Measured T_{mrt} on Jan.15. Isolated points are extracted from simulation results, while continuous curves are from measurement data using a 40 mm grey globe thermometer.
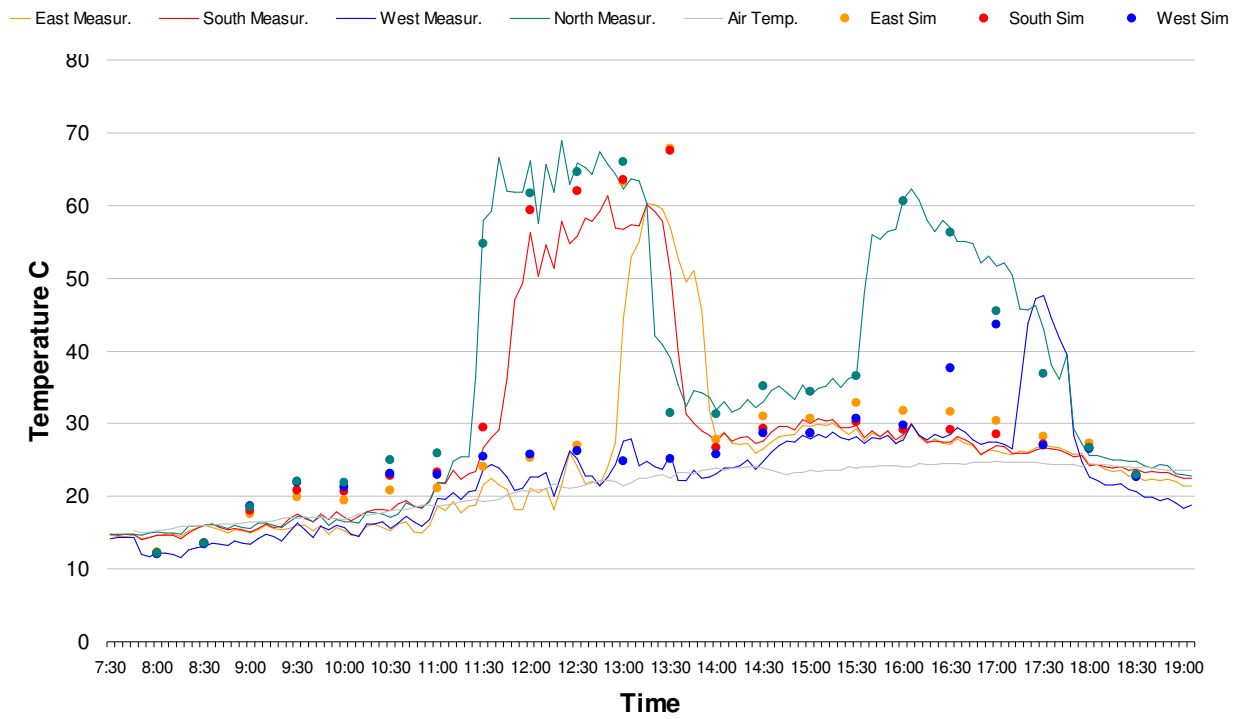
Figure 13. Predicted and Measured T_{mrt} on Mar.21. Isolated points are extracted from simulation results, while continuous curves are from measurement data using a 40 mm grey globe thermometer.